Influence of groundwater flow on thermochronometer-derived exhumation rates in the central Nepalese Himalaya

David M. Whipp, Jr.
Todd A. Ehlers
Department of Geological Sciences, University of Michigan, Ann Arbor, Michigan 48109, USA

ABSTRACT

Mountain topography creates variations in water-table elevation that drive groundwater flow. Consequently, advective heat transport by topography-driven fluid flow can modify the crustal thermal field and bias exhumation rates calculated from thermochronometer data. Although previous studies have considered the thermal effects of fluid flow, none has quantified the influence on thermochronometer ages. We use a steady-state three-dimensional coupled hydraulic thermokinematic finite-element model to simulate the influence of fluid flow on exhumation rates derived from thermochronometer data in the Nepalese Himalaya. Local hot springs suggest substantial heat transport by fluid flow and are adjacent to apatite fission-track samples. Model hydraulic conductivity controls the rate of fluid flow, and values characteristic of fractured rock (>>10^{-9} m/s) yield a fluid advection–dominated thermal field. Hydraulic conductivity is estimated by minimizing the misfit between predicted and observed hot spring thermal power. The best-fit hydraulic conductivity value of ~5×10^{-7} m/s produces a fluid advection–dominated thermal field and older predicted apatite fission-track ages. To fit the observed age-elevation relationship, model-predicted ages require denudation rates that are ~5 mm/yr, ~200% higher than predictions from thermal models that do not simulate fluid flow. Thus, true exhumation rates can be substantially underestimated in orogenic systems where fluid advection is significant.

Keywords: thermochronology, fluid flow, exhumation, numerical modeling, Himalaya.

INTRODUCTION

Surface heat-flow studies suggest that advective heat transport by groundwater flow perturbs the background conductive thermal state of the crust (e.g., Van Orstrand, 1934). Mountain topography produces differences in hydraulic head (e.g., Hubbert, 1940), driving groundwater flow that captures heat from the surrounding bedrock. The water then returns to the surface as warm springs within valleys and modifies the crustal thermal field (Fig. 1). Previous two- and three-dimensional (2-D, 3-D) thermokinematic modeling studies have shown how denudation, surface topography, exhumation trajectory, and topographic evolution affect the subsurface thermal field and predicted mineral cooling ages (Stüwe et al., 1994; Mancktelow and Grasemann, 1997; Ehlers and Farley, 2003; Braun and van der Beek, 2004). Furthermore, 2-D coupled hydrologic-thermal models show modification of the crustal thermal field by topography-driven fluid flow (Smith and Chapman, 1983; Forster and Smith, 1989; Person and Garven, 1994). As noted by Ehlers (2005) and Dempster and Persano (2006), the influence of topography-driven fluid flow on thermochronometer data is seldom considered and poorly quantified.

This work complements previous studies by quantifying the thermal effect of fluid flow on the exhumation histories determined from low-temperature thermochronometer data. We present results from a 3-D coupled hydrologic, thermal, and kinematic model used to predict mineral cooling ages as a function of advective and conductive heat transfer, topography, exhumation rate, and material properties. Predicted apatite fission-track (AFT) ages and hot spring thermal power are compared to observed values from the Marsyandi drainage in central Nepal (Evans et al., 2004; Blythe et al., 2007).

NEPALESE HIMALAYAN GEOLOGY, FLUID FLOW, AND COOLING AGES

Indo-Tibetan convergence in the Nepalese Himalaya during late Miocene–Holocene time is thought to occur dominantly on two major thrusts, the Main Frontal thrust (MFT) and Main Central thrust (MCT) (e.g., Lavé and Avouac, 2000; Hodges et al., 2004), which separate lithostratigraphic units with different hydro-thermo-physical properties. Fractured igneous and upper amphibolite facies metamorphic rocks of the Greater Himalayan Sequence (GHS) are in the hanging wall of the MCT, structurally overlain by the sedimentary rocks of the Tibetan Sequence. Lower grade metasedimentary rocks of the Lesser Himalayan Sequence (LHS) are in the MCT footwall, and the crystalline Indian shield is subducted beneath the Himalaya (e.g., Gansser, 1964).

Evans et al. (2004) compiled a map of hot spring locations within the GHS and LHS in central Nepal, including four springs located within the Marsyandi River valley (Fig. 2). They noted, however, that there may be many unmapped hot springs within the area, including the Nyadi River valley within our study area. They used a geochemical tracer (Ge concentrations) to calculate hot spring input to the Marsyandi River, finding a total hot spring discharge of 330 L/s, or 0.16% of the Marsyandi River discharge [see the GSA Data Repository[1] and Evans et al. (2004) for calculation details]. The high average spring temperature (~51 °C) reflects heat advected from the surrounding rock.

Mapped hot springs in the Marsyandi River valley are adjacent to AFT samples and may have affected their cooling history (Huntington et al., 2006; Blythe et al., 2007). AFT ages reflect the time since cooling below an effective closure temperature of ~100–140 °C for cooling rates of 2–100 °C/m.y. (e.g., Ketcham et al., 1999). This study focuses on a subset of nine samples along a vertical transect to Nagi Lek peak (Fig. 2). AFT ages range from ca. 0.5 to 1.6 Ma over ~3 km of elevation, and the steep slope of the data regression line reflects rapid exhumation. Previous thermokinematic models (without fluid flow) of Whipp et al. (2007), using the AFT data of Blythe et al. (2007), constrained the denudation rates in this region to 1.8–5.0 mm/yr over the past ~3 m.y.

NUMERICAL MODEL

Thermochronometer data are sensitive to the thermal effects of faulting, denudation, topography, and groundwater flow (e.g., see review in Ehlers, 2005). To address these complexities, we use the 3-D coupled thermokinematic finite-element model of Whipp et al. (2007) with the addition of a coupled hydrologic model (see approach of Kohl et al., 2001). The model free parameters are the fault kinematics and hydraulic conductivity (K). The model domain is 84 × 140 × 50 km and large enough to prevent the boundary conditions from biasing the fluid flow and predicted ages. The upper surface is derived from a 250 m digital elevation model. The coupled hydraulic thermokinematic model generates a steady-state thermal solution for this crustal block. A steady-state calculation is used because previous studies have shown that rapidly eroding regions will reach 90% of steady state at AFT closure depths in <5 m.y. (e.g., Stüwe

[1]GSA Data Repository item 2007204, numerical model setup and thermal power calculations, is available online at www.geosociety.org/pubs/ft2007.htm, or on request from editing@geosociety.org or Documents Secretary, GSA, P.O. Box 9140, Boulder, CO 80301, USA.

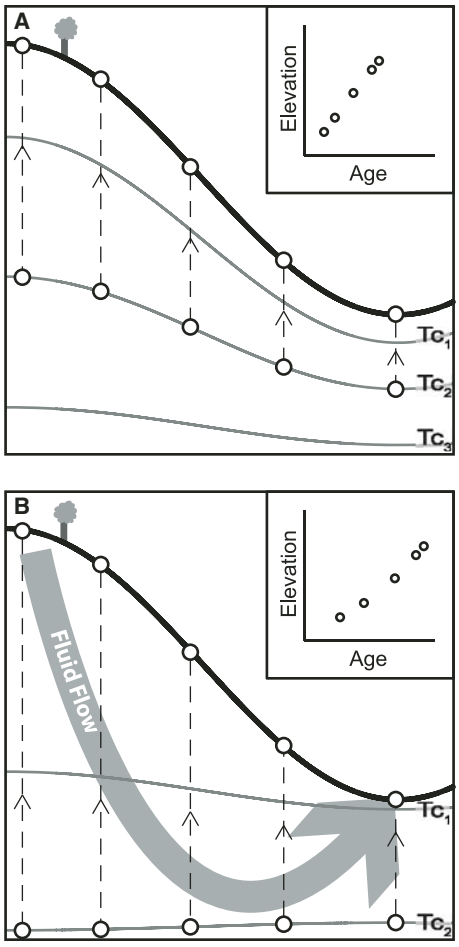

Figure 1. Schematic topographic cross sections showing thermal effects of topography and groundwater flow. Surface topography (thick black line) affects the position of isotherms (thin black lines) and the thermal history recorded in rock samples (white circles) cooling through closure temperatures Tc_1–Tc_3. Insets show distribution of sample ages as function of elevation. A: Thermal field is dominated by erosional advection and heat conduction, and sample ages plot in a straight line on the inset plot. B: Gravity and lateral pressure gradients drive groundwater flow from high to low elevation, leading to heat transfer by fluid advection. This process perturbs closure temperature isotherms, and generates ages that are older and follow curved age-elevation trends.

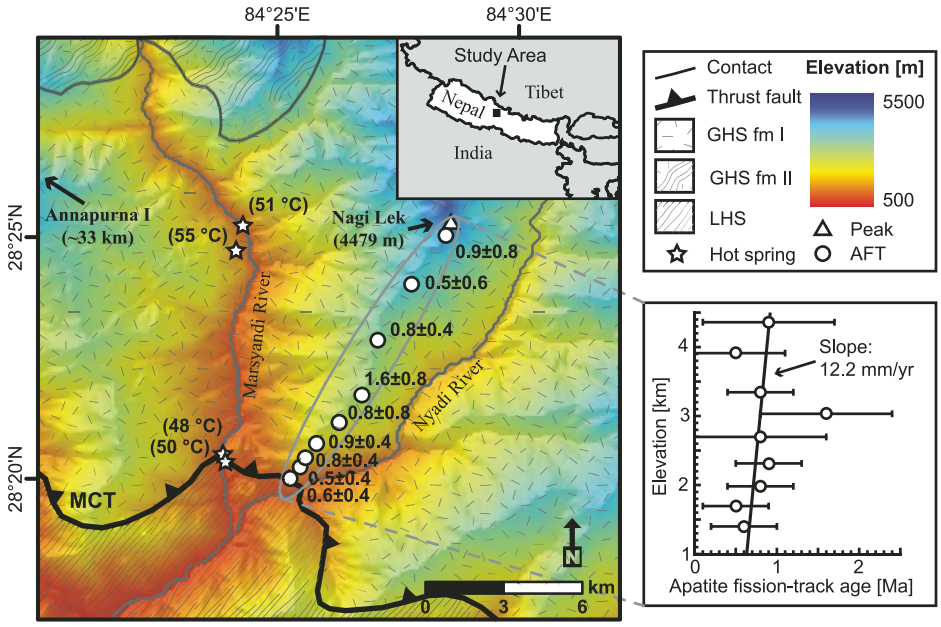

Figure 2. Shaded relief digital elevation model (DEM) of study region in central Nepal with thermochronometer samples, hot spring locations, and major lithostratigraphic units. Apatite fission-track samples (AFT, white circles) are located along Nagi Lek ridge, between Marsyandi and Nyadi Rivers, and adjacent to mapped hot spring locations (white stars). Note that the lack of mapped hot springs in the Nyadi River valley does not preclude their existence. Major thrust fault in the study area (MCT, Main Central thrust) separates Greater Himalayan sequence (GHS) from Lesser Himalayan sequence (LHS). GHS formation I is predominantly biotite-muscovite gneiss, formation II is mainly calc-silicate gneiss, and the map section of LHS is dominantly schists and phyllites. DEM is 250 m resolution resampled from 90 m U.S. Defense Mapping Agency data. Lithostratigraphic units and faults are from Searle and Godin (2003) and Colchen et al. (1986). Outer plot: sample ages with 2σ uncertainties as function of elevation with weighted regression line through the data.

et al., 1994). Particles coincident with the sample locations are tracked through the model to produce time-temperature histories and predict AFT ages using a cooling-rate–dependent age prediction algorithm. We conducted 50 simulations to explore the influence of *K* and fault kinematics on thermochronometer ages. Details on the numerical model and figures illustrating the model domain and fluid flow pathways can be found in the GSA Data Repository (see footnote 1).

The thermokinematic model simulates erosional exhumation of material carried by the MFT and MCT. The MFT and MCT are active at overthrusting rates of 2–8 and 1–4 mm/yr, respectively, generating denudation rates of 1.3–5.0 mm/yr (Whipp et al., 2007). The remainder of the 20 mm/yr of Indo-Tibetan convergence is accommodated by subduction of the Indian shield (e.g., Larson et al., 1999). The model topography is in steady state, which is the simplest assumption because the AFT data are likely most sensitive to variations in the short-wavelength mountain-valley topography dictated by the river locations, thought to have followed similar paths for several million years (e.g., Gupta, 1997). Although relief may have changed, we have no clear data on relief changes.

Hydraulic conductivity is the free parameter in the hydrologic model and controls the rate of fluid flow. The water-table elevation drives fluid flow and is set to mimic topography as an approximation of the true water-table geometry. *K* decreases quasi-exponentially with depth from sequence-specific maxima, following the permeability trend observed in borehole measurements in crystalline rock. *K* is fixed at 10^{-12} m/s below the approximate brittle-ductile transition, as suggested by studies of geothermal data and metamorphic systems (Ingebritsen and Manning, 1999, and references therein). *K* is recalculated in each model time step to account for pressure- and temperature-dependent fluid density, and temperature-dependent fluid viscosity (Phillips et al., 1981; Smith and Chapman, 1983). We recognize that smaller-scale variations in *K* may exist with lithology or in fault zones, and that localized areas with very high *K* may have significant thermal effects. However, we do not model this behavior because only some of the observed hot springs are coincident with mapped fault traces (Fig. 2), spring locations vary over much shorter time scales than our cooling ages integrate, and the stress state and mineral precipitation in fault zones can both increase and decrease *K* (Hickman et al., 1995).

RESULTS AND DISCUSSION

We focus on three important questions related to groundwater flow and thermochronometer ages. (1) What is the threshold *K* value above which fluid flow modifies thermochronometer ages beyond typical sample uncertainties? (2) How can hot spring thermal power measurements be used to quantify *K*? (3) How much does fluid flow influence interpreted exhumation rates relative to commonly used thermal models that ignore groundwater flow? We address

each of these questions by presenting results for a subset of simulations. Note that our use of a steady-state thermal solution likely produces the maximum effect of groundwater flow.

First, we explored the range of K values in the GHS representative of fractured metamorphic rock to unfractured crystalline rock (10^{-4} and 10^{-12} m/s; Freeze and Cherry, 1979, p. 29). These simulations used a constant denudation rate of 2.5 mm/yr and K was the only model free parameter. K has a strong influence on the thermal field because increased downward fluid flow depresses the near-surface isotherms, counteracting the effects of erosional heat advection (Fig. 3A). At K values of ~10^{-12} m/s, erosional advection and heat conduction dominate advective heat transport by fluid flow, whereas for K values of ~5×10^{-7} m/s, fluid-driven advection becomes the principal heat transfer process modifying the thermal field. A K value of ~10^{-9} m/s marks the threshold value, above which fluid advection dominates, and below which erosional advection and conduction dominate the thermal field (see also Forster and Smith, 1989). A vertical temperature profile in the middle of the Nagi Lek ridge shows a temperature difference of ~75 °C at −10 km depth for high K values (Fig. 3A); the difference decreases to <5 °C at −50 km depth. Thus, in models dominated by fluid-advective heat transfer, low-temperature thermochronometer samples would travel longer distances from their closure isotherms to the surface, generating older predicted ages (Fig. 3B). For example, the predicted AFT ages in the fluid-advective models increase by ~1.8 m.y. relative to the non-fluid-advective models. The fluid-advective-model–predicted ages also have a shallower slope on an age versus elevation plot and provide a poor fit to the observed AFT data.

Second, we compare the modeled and observed thermal power of fluids in the Marsyandi River catchment to determine the range of K values applicable to the study area. Thermal power provides a means for quantifying advective heat transport by groundwater flow. Thermal power of the Marsyandi hot springs is calculated following the method outlined by Ehlers and Chapman (1999). We use data collected from four hot springs in the Marsyandi River valley (Tables 2 and 6 of Evans et al., 2004). Evans et al. (2004) showed that Ge/Si ratios could be used to calculate hot spring flux in central Nepal with a simple end-member mixing equation. The total observed thermal power for the hot springs draining into the Marsyandi River is 61.4 ± 36.3 MW; the uncertainty reflects the standard deviation of Ge/Si in the measured springs. Predicted thermal power is calculated from fluids flowing out of the upper model surface using three different sets of assumptions to quantify the range of thermal power (see footnote 1).

The resulting range of predicted thermal power output shows a strong positive correlation with K (Fig. 4A). Only models with K values of ~$1–8 \times 10^{-7}$ m/s have sufficient fluid flow to generate the observed range of thermal power. Thus, advective heat transport by fluid flow may be the dominant heat transfer mechanism in this area. The fluid-advective model K value (5×10^{-7} m/s) is within the range constrained by the observed thermal power (dashed line in Fig. 4A), suggesting that fluid-advective models should be used to determine denudation rates from the AFT data.

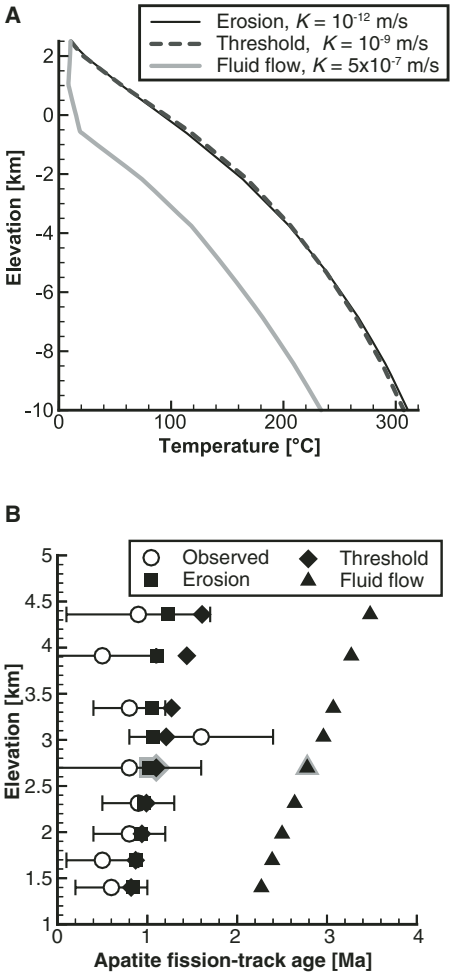

Figure 3. Influence of variable hydraulic conductivity (K) on geothermal gradients and thermochronometer ages from the Nagi Lek transect. A: Variation in model temperature as function of depth for models with K values that produce thermal fields dominated by erosional advection and conduction (erosion, black solid line) and fluid advection (fluid flow, gray solid line). Threshold geotherm (threshold, dashed gray line) is from a model thermal field that is neither non-fluid advective nor fluid advective. B: Apatite fission-track data with 2σ uncertainties (white circles) and predicted ages from non-fluid-advective (black squares), fluid-advective (black triangles), and threshold (black diamonds) models. Denudation rate is 2.5 mm/yr for all simulations. Symbols outlined in gray denote location of temperature-depth profiles shown in A. Shallow age-elevation trend and older ages in B, and depressed geothermal gradient in A from the fluid-advective model (black triangles, solid gray line), show the effect of groundwater flow.

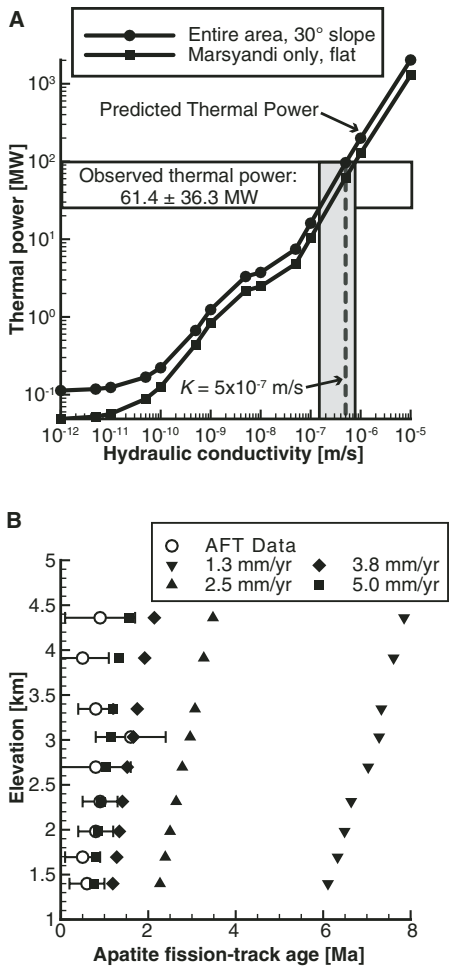

Figure 4. Influence of denudation rate and hydraulic conductivity (K) on thermal power and thermochronometer ages. A: Model-predicted thermal power at denudation rate of 2.5 mm/yr as function of K calculated from models using fluid fluxes from the entire model domain with assumed 30° hillslope angle (black line with black circles) or only Marsyandi River drainage basin and zero slope (black line with black squares). Calculation details are in GSA Data Repository (see text footnote 1). The observed thermal power (white box) constrains the model K values; only models with K value within gray shaded box produce observed thermal power. B: Observed apatite fission-track (AFT) ages (white circles) with 2σ uncertainties and predicted ages for fluid-advective models that have denudation rates of 1.3 (black inverted triangles), 2.5 (black upright triangles), 3.8 (black diamonds), and 5.0 mm/yr (black squares). Rapid denudation rates are required for the fluid-advective model predicted ages to fit the data. Predicted AFT ages are from model with $K = 5 \times 10^{-7}$ m/s (dashed gray line in A).

Third, we investigated the influence of groundwater flow on interpreted exhumation rates with a suite of simulations that fixed K at the fluid-advective value (5×10^{-7} m/s) while varying the denudation rate to fit the observed cooling ages (Fig. 4B). Groundwater flow leads to an increase in the interpreted exhumation rate relative to rates determined from thermal models that do not include groundwater flow. For example, the best-fit non-fluid-advective-model–predicted ages presented in Figure 3B had a denudation rate of 2.5 mm/yr, but predicted ages from a fluid-advective model ($K = 5 \times 10^{-7}$ m/s) produce a poor fit to observed ages at that denudation rate (Fig. 4B, upright triangles). However, increasing the denudation rate to 5.0 mm/yr produces a data fit that is as good as the non-fluid-advective model with a denudation rate of 2.5 mm/yr (cf. Figs. 3B and 4B).

CONCLUSIONS

In this example from the central Nepalese Himalaya, the thermal-power–constrained hydraulic conductivity is high and shows that the denudation rate needed to fit the observed AFT data must be ≥200% larger than that calculated from models that ignore the role of fluid flow. Note, however, that the magnitude of the effect of fluid flow may vary spatially depending on whether valleys or ridges are sampled. This example has extreme topographic relief, but the thermal effects of groundwater flow in other orogens with less relief and precipitation may still be substantial and should be considered (e.g., Saar and Manga, 2004). Furthermore, the downward flow of groundwater may counteract the topographic effects on effective closure isotherms and yield exhumation rates that are similar to those calculated from the slope of a linear regression through the data in an age-elevation plot. Unfortunately, this potential agreement would be mere coincidence because many of the underlying assumptions would be invalid, so it is advisable to utilize numerical models to quantify the dominant influences on the thermal field.

ACKNOWLEDGMENTS

We thank Matt Evans, Louis Derry, and Ye Zhang for thoughtful discussions during the early stages of this study. Tim Dempster, Neil Mancktelow, and an anonymous reviewer provided constructive reviews. This study was supported by National Science Foundation grants EAR-9909647 and EAR-0409289 to Ehlers.

REFERENCES CITED

Blythe, A.E., Burbank, D.W., Carter, A., Schmidt, K., and Putkonen, J., 2007, Plio-Quaternary exhumation history of the central Nepalese Himalaya: 1. Apatite and zircon fission-track and apatite [U-Th]/He analyses: Tectonics, v. 26, TC3002, doi: 10.1029/2006TC001990.

Braun, J., and van der Beek, P., 2004, Evolution of passive margin escarpments; what can we learn from low-temperature thermochronology?: Journal of Geophysical Research, v. 109, p. F04009, doi: 10.1029/2004JF000147.

Colchen, M., Le Fort, P., and Pecher, A., 1986, Recherches géologiques dans l'Himalaya du Nepal, Annapurna; Manaslu, Ganesh Himal; notice de la carte géologique au 1/200 000: Poitiers, France, Centre National de Recherches Scientifiques, scale 1:200,000.

Dempster, T.J., and Persano, C., 2006, Low-temperature thermochronology; resolving geotherm shapes or denudation histories?: Geology, v. 34, p. 73–76, doi: 10.1130/G21980.1.

Ehlers, T.A., 2005, Crustal thermal processes and the interpretation of thermochronometer data: Reviews in Mineralogy and Geochemistry, v. 58, p. 315–350, doi: 10.2138/rmg.2005.58.12.

Ehlers, T.A., and Chapman, D.S., 1999, Normal fault thermal regimes; conductive and hydrothermal heat transfer surrounding the Wasatch fault, Utah: Tectonophysics, v. 312, p. 217–234, doi: 10.1016/S0040–1951(99)00203–6.

Ehlers, T.A., and Farley, K.A., 2003, Apatite (U-Th)/He thermochronometry; methods and applications to problems in tectonic and surface processes: Earth and Planetary Science Letters, v. 206, p. 1–14, doi: 10.1016/S0012–821X(02)01069–5.

Evans, M.J., Derry, L.A., and France-Lanord, C., 2004, Geothermal fluxes of alkalinity in the Narayani river system of central Nepal: Geochemistry, Geophysics, Geosystems, v. 5, p. 21.

Forster, C.B., and Smith, L., 1989, The influence of groundwater flow on thermal regimes in mountainous terrain; a model study: Journal of Geophysical Research, B, Solid Earth and Planets, v. 94, p. 9439–9451.

Freeze, R.A., and Cherry, J.A., 1979, Groundwater: Englewood Cliffs, New Jersey, Prentice-Hall, Inc., 604 p.

Gansser, A., 1964, Geology of the Himalayas: London, Wiley Interscience, 289 p.

Gupta, S., 1997, Himalayan drainage patterns and the origin of fluvial megafans in the Ganges foreland basin: Geology, v. 25, p. 11–14, doi: 10.1130/0091–7613(1997)025<0011:HDPATO>2.3.CO;2.

Hickman, S., Sibson, R.H., and Bruhn, R., 1995, Introduction to special section; mechanical involvement of fluids in faulting: Journal of Geophysical Research, v. 100, p. 12,831–12,840, doi: 10.1029/95JB01121.

Hodges, K.V., Wobus, C.W., Ruhl, K., Schildgen, T., and Whipple, K.X, 2004, Quaternary deformation, river steepening, and heavy precipitation at the front of the Higher Himalayan ranges: Earth and Planetary Science Letters, v. 220, p. 379–389, doi: 10.1016/S0012–821X(04)00063–9.

Hubbert, M.K., 1940, The theory of ground-water motion: Journal of Geology, v. 48, p. 785–944.

Huntington, K.W., Blythe, A.E., and Hodges, K.V., 2006, Climate change and late Pliocene acceleration of erosion in the Himalaya: Earth and Planetary Science Letters, v. 252, p. 107–118, doi: 10.1016/j.epsl.2006.09.031.

Ingebritsen, S.E., and Manning, C.E., 1999, Geological implications of a permeability-depth curve for the continental crust: Geology, v. 27, p. 1107–1110, doi: 10.1130/0091–7613(1999)027<1107:GIOAPD>2.3.CO;2.

Ketcham, R.A., Donelick, R.A., and Carlson, W.D., 1999, Variability of apatite fission-track annealing kinetics III, Extrapolation to geological time scales: American Mineralogist, v. 84, p. 1235–1255.

Kohl, T., Signorelli, S., and Rybach, L., 2001, Three-dimensional (3-D) thermal investigation below high Alpine topography: Physics of the Earth and Planetary Interiors, v. 126, p. 195–210, doi: 10.1016/S0031–9201(01)00255–2.

Larson, K.M., Buergmann, R., Bilham, R., and Freymueller, J.T., 1999, Kinematics of the India-Eurasia collision zone from GPS measurements: Journal of Geophysical Research, B, Solid Earth and Planets, v. 104, p. 1077–1093, doi: 10.1029/1998JB900043.

Lavé, J., and Avouac, J.P., 2000, Active folding of fluvial terraces across the Siwaliks Hills, Himalayas of central Nepal: Journal of Geophysical Research, B, Solid Earth and Planets, v. 105, p. 5735–5770, doi: 10.1029/1999JB900292.

Mancktelow, N.S., and Grasemann, B., 1997, Time-dependent effects of heat advection and topography on cooling histories during erosion: Tectonophysics, v. 270, p. 167–195, doi: 10.1016/S0040–1951(96)00279-X.

Person, M., and Garven, G., 1994, A sensitivity study of the driving forces on fluid flow during continental-rift basin evolution: Geological Society of America Bulletin, v. 106, p. 461–475, doi: 10.1130/0016–7606(1994)106<0461:ASSOTD>2.3.CO;2.

Phillips, S.L., Igbene, A., Fair, J.A., Ozbek, H., and Tavan, M., 1981, A technical databook for geothermal energy utilization: Berkeley, California, Lawrence Berkeley Laboratory Report 12810, 55 p.

Saar, M.O., and Manga, M., 2004, Depth dependence of permeability in the Oregon Cascades inferred from hydrogeologic, thermal, seismic, and magmatic modeling constraints: Journal of Geophysical Research, B, Solid Earth and Planets, v. 109, p. 19.

Searle, M.P., and Godin, L., 2003, The South Tibetan detachment and the Manaslu Leucogranite; a structural reinterpretation and restoration of the Annapurna-Manaslu Himalaya, Nepal: Journal of Geology, v. 111, p. 505–523, doi: 10.1086/376763.

Smith, L., and Chapman, D.S., 1983, On the thermal effects of groundwater flow—1. Regional scale systems: Journal of Geophysical Research, v. 88, p. 593–608.

Stüwe, K., White, L., and Brown, R., 1994, The influence of eroding topography on steady-state isotherms; application to fission track analysis: Earth and Planetary Science Letters, v. 124, p. 63–74, doi: 10.1016/0012–821X(94)00068–9.

Van Orstrand, C.E., 1934, Temperature gradients, *in* Wrather, W.E., and Lahee, P.H., eds., Problems in petroleum geology: Tulsa, Oklahoma, American Association of Petroleum Geologists, p. 1073.

Whipp, D.M., Jr., Ehlers, T.A., Blythe, A.E., Huntington, K.W., Hodges, K.V., and Burbank, D.W., 2007, Plio-Quaternary exhumation history of the central Nepalese Himalaya: 2. Thermokinematic and thermochronometer age prediction model: Tectonics, v. 26, TC3003, doi: 10.1029/2006TC001991.

Manuscript received 9 February 2007
Revised manuscript received 27 April 2007
Manuscript accepted 3 May 2007

Printed in USA